Progress in the Conceptual Design of the Helical Fusion Reactor FFHR-d1

Nagato Yanagi[1], Takuya Goto[1], Junichi Miyazawa[1], Hitoshi Tamura[1], Yoshiro Terazaki[1], Satoshi Ito[2], Teruya Tanaka[1], Hidetoshi Hashizume[2], and Akio Sagara[1]

[1]National Institute for Fusion Science, 322-6 Oroshi-cho, Toki, Gifu 509-5292, Japan

[2]Department of Quantum Science and Energy Engineering, Graduate School of Engineering, Tohoku University, Sendai, Miyagi 980-8579, Japan

E-mail of main author: yanagi@nifs.ac.jp

Abstract

The LHD-type helical fusion reactor FFHR has been studied to realize steady-state fusion power generation without a need for current drive and free from disruption. The conceptual design studies of FFHR are steadfastly progressing based on the presently ongoing experiments in the Large Helical Device (LHD). In order to enhance the attractive features of the base option of FFHR-d1A, which is similar to LHD, configuration optimization is being considered for FFHR-d1C. Slight modification of the helical coil trajectory gives an improved condition both for the plasma confinement and the MHD stability. In order to overcome the difficulty for construction and maintenance associated with the three-dimensional structure, innovative ideas are being explored for the superconducting magnet, divertor, and blanket. For the superconducting helical coils, the joint-winding method confirms a fast manufacturing process. The helical divertor is reexamined and practical feasibility is discussed. The maintenance method of the helical divertor and the helically-segmented breeder blanket is a serious issue and a plausible solution is proposed.

Key Words

helical fusion reactor; FFHR; heliotron; configuration optimization; high-temperature superconductor; helical divertor; blanket maintenance; Aquarium method

1. Introduction

Conceptual design studies of the helical fusion reactor FFHR-d1 have been progressing at National Institute for Fusion Science (NIFS) [1-3]. The FFHR design has been continued since its start in 1998 [4] as the world's longest fusion reactor design [5] on the basis of the fruitful experimental results obtained in the Large Helical Device (LHD) [6, 7]. The LHD has started the deuterium experiment in 2017 [8] and confinement improvement is being examined. The FFHR has the heliotron magnetic configuration, which is inherently steady-state. No major disruption is expected and there is no need for current drive [9, 10]. This is similar to other stellarator systems in which the reactor designs are also progressing by employing various configurations [11, 12]. A self-ignition or self-sustained burn is theoretically foreseen because of there being no requirement for current drive [1, 10]. (The power requirement for all the ancillary systems, such as the cryogenic system, should be separately counted.) Due to its large aspect ratio and the resulting high ratio of surface area to plasma volume, long-life blanket is expected due to the lower neutron wall loading compared

to the case of lower aspect ratio devices. One of the most important features of the heliotron magnetic configuration is found in its helical built-in divertor.

The heliotron magnetic configuration of FFHR-d1 is similar to that of LHD. A pair of continuously-wound helical coils has a toroidal pitch number of 10 and two pairs of Outer Vertical (OV) and Inner Vertical (IV) coils are located above and below the helical coils to adjust the vertical field. In order to obtain large port areas for the maintenance works of in-vessel components, such as blankets and divertors, the Inner Shaping (IS) coils equipped in LHD are omitted in the present design. The major radius, R, of the helical coils is 15.6 m, which is four times that of LHD (R = 3.9 m). A toroidal magnetic field of 4.7 T (averaged in the toroidal direction) is produced at the geometrical center of the helical coils. In the standard operation scenario of FFHR-d1, the magnetic axis is shifted inward at R = 14.4 m to secure good energy confinement characteristics [2], which corresponds to the standard configuration of LHD at R = 3.6 m. The overall stored magnetic energy reaches 169 GJ. Under these conditions, a self-ignited fusion power of 3 GW is expected to be produced. Figure 1 shows a schematic comparison between LHD and FFHR-d1.

In order to secure the design foundation, a multi-path strategy is employed [3]. The FFHR-d1A is defined as the base option for promoting the 3D engineering design, having the major and minor radius of the helical coils of R_c = 15.6 m and a_c = 3.744 m, respectively. Here the helical pitch parameter γ_c is defined as

$$\gamma_c = \frac{m}{l}\frac{a_c}{R_c}, \qquad (1)$$

where m =10 and l =2 are the toroidal and poloidal pitch numbers, respectively. For FFHR-d1A, γ_c is 1.20, which was changed from the previous value of 1.25 for FFHR-d1 having a_c = 3.9 m. This is for the purpose of improving the confinement characteristics by reducing the Shafranov shift. Figure 2 shows the vacuum magnetic surfaces of FFHR-d1A at two toroidal cross-sections. Figure 3 shows a plan view of the magnet system. An increase of toroidal magnetic field by 20% to 5.6 T is proposed as FFHR-d1B, to secure the self-ignition capability at 3 GW fusion power. The increase of magnetic field makes the mechanical stresses larger along with the increase of magnetic stored energy (by 40%) which makes the structural design and material selection more difficult. The numerical analysis using the Finite Element Method (FEM) has been conducted using the ANSYS 16.1 code to evaluate the mechanical stress caused by the electromagnetic forces. The von Mises stress is ~660 MPa in FFHR-d1A [13, 14], and thus, it reaches the level of ~950 MPa for FFHR-d1B. We note that this situation is still acceptable both by using the high-strength stainless steels developed for ITER [15] with a yield strength of ~1000 MPa at the cryogenic temperature of ~4 K and by having some structural modification with the supporting structure to ease the stress concentration. However, to have a larger safety margin in the mechanical property, in this paper, the FFHR-d1C option is proposed as a flexible design with configuration optimization so that the required magnetic field could be on the same level as that for FFHR-d1A. We note that slight modifications of the helical coils and vertical field coils could also provide many engineering benefits.

For the engineering design of FFHR-d1C, several innovative ideas have been proposed for the following three purposes: (1) to overcome the difficulties related with the construction and maintenance of three-dimensionally complicated large structures, (2) to enhance the passive safety, and (3) to improve the plant efficiency. In this paper, discussion is focused on (1) for the superconducting helical coils, the helical divertor, and the helically-segmented breeder

blanket. The helical divertor in particular is reexamined. A new proposal is given regarding the maintenance work under intense gamma radiation environment.

2. Configuration optimization of FFHR-d1

For FFHR-d1B (higher magnetic field version of FFHR-d1A), the operation point has been explored using a design integration systems code, HELIOSCOPE [16] that incorporates the "Direct Profile Extrapolation" (DPE) method [17] for predicting the plasma parameters based on the experimentally obtained data in LHD plasmas. An integrated physics analysis using the HELIOSCOPE determines a self-consistent operation point that assures the energy multiplication factor of $Q \sim 10$ [18]. The confinement improvement in the ongoing deuterium plasma experiments in LHD, if confirmed, should enhance the Q-value. However, the limit is given also by the MHD stability. The achievable beta value is examined for the pressure driven instability using the Mercier stability criterion. In this respect, the improvement of the plasma performance is preferred.

To accommodate this situation, and to improve the Q-value, so that the self-ignition is finally achieved, the configuration optimization is considered as a useful option. In this paper, FFHR-d1C is proposed as a flexible design with configuration optimization. Slight modifications of the helical coils and vertical field coils could provide many engineering benefits. One possibility of FFHR-d1C is to incorporate the shift-optimized configuration proposed by S. Okamura [19, 20] by adjusting the essential Fourier modes that define the outermost magnetic surface, or the plasma boundary. This FFHR-d1C-SO configuration has favorable features of both inward and outward shifted configurations. It is expected that the Shafranov shift with an increase of the plasma beta becomes smaller than the case with the FFHR-d1A (similar to the LHD) configuration. It is also shown that the helical ripples are also smaller, which may lead to smaller neo-classical diffusion.

This configuration is realized by employing a modified winding law of the helical coils with trajectories around a horizontally elongated ellipse. Note that the helical coils of LHD are wound on a circular torus.

More specifically, the trajectory of the first helical coil (of a pair of helical coils) is defined as

$$\theta = -\left(\frac{m}{l}\phi + \alpha \sin \frac{m}{l}\phi \right), \tag{2}$$

$$r_c = a_c \frac{\left(1+\varepsilon_a+\varepsilon_b\right)}{\sqrt{\cos^2\theta\left(1+\varepsilon_b\right)^2+\sin^2\theta\left(1+\varepsilon_a\right)^2}} \tag{3}$$

where θ and ϕ are the poloidal and toroidal angles, respectively, r_c is the minor radius of the helical coils, a_c is the original minor radius of the helical coils with a circular cross-section, ε_a and ε_b are the ellipticity in the horizontal and vertical directions, respectively. For the second helical coil, ϕ is shifted by 180 degrees. We note that the helical coils of the FFHR-series are all wound in the right-handed screw fashion (like LHD). For FFHR-d1A, α is 0.1, and ε_a and ε_b are both zero (like LHD). For FFHR-d1C-SO, α is -0.02 and ε_a = 0.05 (whereas ε_b = 0), and thus, the helical coil has a slightly larger minor radius in the horizontal direction.

In the FFHR-d1A configuration, the "blanket space" Δ_{cp} (the distance between the innermost layer of the helical coil windings and the ergodic layer outside the last closed flux surface) is found to be very tight at 950 mm on the inboard side of the torus. It was recently proposed that γ_c could be flexibly adjusted by employing a pair of sub helical coils located outside the main helical coils [21]. The sub-helical coils are presently called NITA (Newly Installed Twist Adjustment) coils. The NITA coils are situated at about two times the minor radius of the main helical coils. An oppositely directed current of -7.7% of the main helical coil current in the NITA coils is effective for enlarging Δ_{cp} to ~1100 mm. Securing a larger space for a thicker shield would lower the neutron flux so that the lifetime of the helical coils is prolonged and the nuclear heating is reduced. The latest design of the FFHR-d1C-SO configuration is determined to also employ a pair of NITA coils. The vacuum magnetic configuration of FFHR-d1C-SO is shown in Fig. 4. Two basic properties of the vacuum magnetic configuration, rotational transform and magnetic well depth, both as a function of the average minor radius, are shown in Fig. 5. We note that the rotational transform is lower than 0.5 at the plasma core. However, its impact on the emergence of a magnetic island could be limited [22]. A further optimization is explored with some deviations from the present configuration and the Q-value will be evaluated in our future studies.

The alpha particle confinement capability in the heliotron reactors has been studied using numerical simulations [23, 24]. A preliminary study for the FFHR-d1C-SO configuration is being performed by employing the guiding center orbit calculation. A calculation result shows that the alpha particle confinement is not very different from that which was obtained for the FFHR-d1A configuration. When alpha particles are emitted from the effective minor radius at the ratio of 0.7 to the last closed flux surface (LCFS), having various pitch angles to magnetic field lines, there are about 20% prompt losses for both configurations. In the present calculation, reentering of particles is assumed, which means that even if particles go out of the LCFS, it is assumed that the particles are not lost immediately and that they will continue their trajectories by reentering the LCFS. A detailed study will be completed and reported in our future studies.

3. Joint-Winding of the FFHR-d1 Helical Coils with HTS Conductors

For the superconducting magnet system of FFHR-d1, the high-temperature superconductor (HTS) using the Rare-Earth Barium Copper Oxide (REBCO) coated conductor tapes is considered [25-28] as an alternative option to the original cable-in-conduit conductor using low-temperature superconducting Nb_3Sn strands [29, 30], which is an extension of the ITER technology. In the present design of the helical coils of FFHR-d1, the number of winding turns is 390 and the conductor current is 94 kA at the maximum magnetic field of 11.8 T [28]. The current density is ~25 A/mm^2 in the winding area. The nominal operation temperature is set at 20 K. In the HTS conductor of a 100 kA current capacity, REBCO tapes are simply stacked and embedded in a copper stabilizer and an outer stainless steel jacket for the mechanical reinforcement. Due to this configuration, this conductor is named STARS (Stacked Tapes Assembled in Rigid Structure). The concept of simple stacking of HTS tapes is in contrast to other approaches for making large-current capacity HTS conductors to be applied to pulsed coils of tokamaks, which includes twisting and transposition of tapes to avoid formation of non-uniform current distribution among tapes and to reduce AC losses. The STARS conductor is expected to be applicable to steady-state DC magnets of helical fusion reactors.

Two prototypes of STARS conductor samples were fabricated and tested in the superconductor testing facility at NIFS equipped with 9-T split-coils [31, 32]. They used 20 and 54 GdBCO tapes (FYSC-SC10 by Fujikura Ltd., tape width: 10 mm, critical current: ~600 A at 77 K, self-field) to ensure the nominal operation current of 30 kA and 100 kA, respectively. Both samples had racetrack shapes and one of the straight sections had a bridge-type mechanical lap joint so that the entire sample formed a short circuit. The sample current was induced by changing the bias magnetic field. For the 100-kA-class sample, the current reached 100 kA at a temperature of 20 K and magnetic field of 5.3 T. At 4.2 K, a 100 kA current was stably sustained for 1 hour by controlling the changing rate of the bias magnetic field. In these samples, a bridge-type mechanical lap joint with a staircase-like structure developed at Tohoku University was applied [33, 34]. The joint resistance was evaluated to be 1.8 nΩ from the measured decay time constant of ~1000 s using the numerically calculated self-inductance of the sample.

The STARS conductor has an internal electrical insulation between the copper stabilizer and the stainless steel jacket. This is for the purpose of welding the neighboring turns of conductors on their stainless steel jackets after winding. As a result, after the winding process, the winding package would resemble that of the ITER TF coils which are equipped with radial plates. By having this configuration, the Vacuum Pressure Impregnation (VPI) process can be skipped. Otherwise, VPI must be applied after the completion of winding by raising the temperature of the entire helical coils up to ~150 centigrade. For the internal electrical insulator, Glass-Kapton-Glass tapes filled with epoxy resin are the conventional choice. An advanced ceramic option will be explored in our future studies to ensure good thermal contact and robustness against neutron irradiation.

Using the HTS conductor, the “joint-winding” has been proposed for the helical coils, which facilitates the fabrication by connecting conductor segments onsite. The concept is summarized in Fig. 6. This is a practical extension of the original ideas regarding the “demountable coil” concept [35, 36]. A one-helical-pitch conductor of ~30 m length could be the basic unit, as was confirmed by 3D printing [37]. The joint process can be performed by lifting the joint section at ~500 mm above the final position in the windings, as the close-up view is shown in Fig. 7. According to our own experience of fabricating a hand-made joint in 3 days (~8 hours of work each day), it is feasible to assume that a joint fabrication (including inspection) is completed with an established procedure in one day (12-16 hours) by skillful workers. Then, the entire onsite winding is expected to be completed in less than 3 years, assuming that four joints (two helical coils in two directions) will be wound in parallel. If one joint is made in one-half day (6-8 hours) using an industrial robot, the entire process will be completed in less than 1.5 years.

According to the joint resistance of 1.8 nΩ measured in the 100-kA-class prototype STARS conductor sample, the joint resistivity is evaluated to be ~15 pΩm^2. This expects the joint resistance in the FFHR-d1 helical coils to be ~1 nΩ at each joint, because of the increase of the surface areas for the joint. Having a 94 kA current, the Joule heating occurs at ~34 kW for the entire helical coils with 3,900 joints. Recently, a new technique for drastically decreasing the joint resistance has been developed [38]. By increasing the temperature to ~100 centigrade during the joint fabrication using single tapes, the joint resistivity was evaluated to be ~3.5 pΩm^2. If this technique can be applied to the 100-kA-class conductor with multi-layers of REBCO tapes, it gives only ~8 kW of joule heating in the entire helical coils, which is ~1/10 of the previous value.

For the HTS magnet design, quench protection, cooling and electromagnetic stress analysis are also important engineering issues. The quench protection scheme using conventional

dump resistors is examined by conducting a hot-spot temperature analysis [39]. The result shows that the current density of 25 A/mm^2 gives a tolerable hot-spot temperature of <200 K. We should note that higher current density gives a higher hot-spot temperature, which makes the quench protection more difficult. In the case of having a higher current density than this, we must adopt some advanced methods, such as an early quench detection or the non-insulation winding method [40].

The cooling scheme using helium gas circulation is examined by a crude analytical estimation [39], which confirms its feasibility with the presently assumed neutron heating. The electromagnetic stress analysis has been progressing with an FEM calculation code and the maximum stress and strain in the coil as well as in the supporting structure are found to be at tolerable levels [13, 14]. Here the maximum tensile strain is found at 0.15%. The multiscale analysis shows that the maximum shear stress of 32 MPa appears in the conductor cross-section. This should happen also at the joint section, which is evaluated to be tolerable [41] using scaled-down sample tests. The increase of the joint resistance is found to be also negligible [42].

It is noted that in addition to the helical coils, other coils in FFHR-d1, the vertical field coils (OV coils and IV coils), NITA coils and corrections coils (such as the RMP coils and HD coils described in the next section) can also be fabricated using the HTS STARS conductors and joint-winding method, if required.

4. Feasibility of the Helical Divertor

4.1 Basic characteristics of the helical divertor

The concept of magnetic confinement by the heliotron configuration was explored from the beginning to equip a "built-in" divertor system [43]. As shown in Fig. 2, a remarkable feature of the heliotron configuration is that clear divertor legs protrude from the confining region and their fundamental structure is determined basically by the helical coil paths. It is noted that this structure is not seriously affected by the plasma beta and/or the toroidal plasma current.

For the helical built-in divertor, the divertor tiles are placed at the backside of the breeder blankets where the incident neutron flux emitted from the core plasma is sufficiently reduced. This is a benefit of the heliotron magnetic configuration which was proposed from the beginning of the concept proposal [44, 45]. This is a tremendous benefit considering the recently recognized problem regarding the heat conductivity degradation by neutron irradiation on tungsten. The neutron flux is calculated by the MCNP code [46] and for the FFHR-d1A configuration, it is evaluated that the fluence may reach >1.6 dpa/year on the inboard side of the torus [47]. We note that a copper-alloy can still be used for cooling pipes if the maximum neutron fluence is limited to be lower than ~1 dpa. If a copper-alloy can be used for cooling pipes, a steady-state heat flux of up to 20 MW/m^2 could still be accommodated by a tungsten tile. If this is not tolerated, the Reduced-Activation Ferritic/Martensitic (RAFM) steel could be the solution, with which the heat flux should be limited to be lower than ~5 MW/m^2. For this reason, it was considered as an option for FFHR-d1A to remove a portion of one of the shell arms to place the divertor tile completely in the backside of the breeder blanket [47]. In this case, the neutron flux could be sufficiently reduced to be an order of magnitude lower. The electromagnetic stress is still accommodated with this modification and the result is not far from the original evaluation in [48]. It is noted

that the configuration of FFHR-d1C-SO shows that the divertors could be better protected from the incident neutron irradiation by blankets than the situation for FFHR-d1A (and B) especially on the inboard side of the torus, as is seen in Fig. 4. In this case, such a cut in the shell arms considered for FFHR-d1A is not necessary.

Regarding the heat flux handling, the helical divertor is supposed to potentially possess large wetted area because of the relatively large major radius and by having a double-null configuration. For FFHR-d1, the total length of the divertor traces is evaluated to be ~900 m for four legs. In the LHD experiments, the effective width of the divertor footprints was observed to be ~20 mm. Therefore, in a crude estimation, we may assume that the corresponding width in FFHR-d1 is four times larger to be ~80 mm. This could be also confirmed by magnetic field-line tracing calculations. We also note that in the heliotron configuration the ergodic layers cover the LCFS before coming to the scrape-off layer. In this situation, we consider that the distribution of field-lines determines the strike points, which might be different from the situation for tokamaks in which the width of a scrape-off layer is supposed to become narrower with a larger plasma size.

Using these values, we obtain an average divertor heat flux of ~8 MW/m^2 for 3 GW fusion power generation (600 MW alpha heating power coming to the divertor region), which seems quite favorable for the divertor engineering design considering the number of difficulties for developing materials to be used under the neutron environment in fusion reactors. However, we should realize that a relatively large toroidal non-uniformity exists with the helical divertor traces, as has been observed in LHD [49, 50]. This may give significantly higher peak heat fluxes at some locations.

In Fig. 2, it is seen for the FFHR-d1 configuration that the divertor legs tend to protrude dominantly at the inboard side of the torus and the strike points are concentrated on this side with the horizontally elongated cross-section of the plasma (at $\phi = 18°$). Whereas much fewer magnetic field-lines come to the inboard side at $\phi = 0°$ with the vertically elongated cross-section and the field-lines hardly come the outboard side at every cross-section. This feature was experimentally observed with the inward shifted configuration in LHD. In the calculations of magnetic field-line tracing, the footprints on the helical divertors can be obtained. In the analysis, the field-line tracing is started just outside the closed magnetic flux surface at every 1° in the toroidal direction and at every 5° in the poloidal direction so that a total of 5184 traces are performed. In Fig. 8, when the field-line crosses the planes indicated by the dashed lines at each toroidal cross-section, the position is collected as a footprint. The toroidal and poloidal angles of the obtained footprints are shown in Fig. 9(a). Two curves are obtained depending on the direction of the magnetic field-line tracing. The number of footprints is then counted along each curve with a 1° toroidal angle pitch, and the fraction is plotted as a histogram in Fig. 9(b) as a function of the toroidal angle φ (defined in Fig. 2). The result shows that the distribution of footprints has a large toroidal non-uniformity. In this plot, the average fraction is given at 1/72 = 0.0139. Thus, we find that from considering the spatially averaged heat flux of ~8 MW/m^2, as described above, the peak heat flux reaches up to ~100 MW/m^2 at $\varphi = 31°$. This level of heat flux is not acceptable and it should be sufficiently reduced. In this case, the width is assumed to be ~80 mm, as described above, all along the divertor traces. We also note that the distribution of footprints changes depending on the magnetic configuration, i.e., by changing the dipole field component (magnetic axis position), quadrupole, and higher components.

Considering this situation, we may need to have radiation dispersion accompanied with plasma detachment to reduce the peak heat flux significantly [51]. However, the compatibility with good core plasma confinement is an important issue to be explored in the future, just like

the situation also for tokamak reactors. Moreover, there remains a great concern that a detachment condition may be terminated abruptly, and then, the attachment condition cannot tolerate the large heat flux even for a short period of time. In this respect, our priority for the FFHR design is to situate the divertor without assuming the detached scenario and radiation dispersion, even though they could be realized in the usual operation.

4.2 Two former proposals to reduce the peak heat flux on the helical divertor

In order to reduce the possible peak heat flux in the helical divertors, two ideas were previously proposed.

One was the strike point sweeping using a pair of auxiliary helical coils, named "Helical Divertor (HD) Coils" [52]. In the LHD experiment, a method of strike point sweeping has been actually tested by changing the vertical magnetic field [53]. This is called the "magnetic-axis swing," since the major radius of the magnetic axis is changed depending on the vertical field. It has been confirmed that this method is actually effective in mitigating the toroidal non-uniformity of heat flux, and it has contributed in achieving the world largest injection energy into the plasma (~1.6 GJ) in the steady-state experiments. Although this scheme is quite useful for LHD with limited heating powers, it may not provide a sufficient capability of heat flux reduction for FFHR with ignited plasmas. The difficulty is that the magnetic configuration is significantly altered to assure sufficient mitigation, but this also changes the fusion output through the change of the plasma volume as well as by the change of confinement characteristics of the bulk plasma and high-energy particles. Note that the outward-shifted configuration is not suitable for the confinement of alpha particles and for the neo-classical transport. Moreover, this scheme of magnetic-axis swing is effective only in the AC mode, which causes AC losses in the superconducting coils. In comparison, the HD coils installed at both sides of the main helical coils (near the divertor strike points) carrying a few percent of the current amplitude of the main helical coils effectively sweep the divertor strike points in the poloidal direction over a width of ~800 mm, which is roughly ten times the originally expected width of strike points. We observe that there is almost no change in the core magnetic surfaces. It is thus noted that there should be almost no effect on the confinement of alpha particles by having these HD coils. It is also evaluated that the thermal fatigue problem associated with the AC operation could be in an acceptable level with a ~0.5 Hz operation. However, the biggest problem with this scheme is that the toroidal non-uniformity still remains. We may consider that the AC losses in the magnet system are relatively small and tolerable. However, some other unforeseen difficulties may arise in the engineering design associated with the AC operation. In this respect, we now consider that the HD coils should be used for the purpose of erosion mitigation rather than heat flux mitigation. This means that a strike point sweeping on divertor plates is performed over a very long period of operation (such as one week or one month). We note that the sweeping makes the entire divertor plate area be fully utilized. This is supposed to be very effective for a long period operation of the helical plasma.

The other idea to reduce the peak heat flux on the divertor was to use RMP (Resonance Magnetic Perturbation) coils to obtain a configuration with a flattened toroidal distribution of strike points [54] so that the peak heat flux may be mitigated. The advantage of this scheme is that it should work in steady-state. In the analysis, 20 RMP coils were installed above and below the vacuum vessel. They are similar to the correction coils installed in LHD, called the "Local Island Divertor (LID)" coils, which are used to control the magnetic islands having the poloidal (m) and toroidal (n) mode numbers, such as $m = 1/n = 1$ and $m = 2/n = 1$ by energizing some of the coils. In the present case, all the 20 coils are energized simultaneously in the same direction so that the mode numbers are $m = 2/n = 10$. We note that if the RMP

coils are to be used also as corrections coils, the current in each coil would have to be individually controlled. Using the RMP coils, the footprints of the divertor legs are obtained in the magnetic field-line tracing in vacuum. Their fraction in every 1° pitch along the toroidal angle is plotted for the case of having the total current of 6 MA in each RMP coil. In this case, it is seen that the peak heat flux can be mitigated. We evaluate that the peak heat flux would become ~1/3. However, this means that the maximum heat flux of ~30 MW/m^2 still comes to the divertor plates. We then considered that it might be possible to reduce these peaks further to ~1/3 by radiation dispersion so that the maximum heat flux would become <10 MW/m^2. Another possibility for a reduction of local heat flux is to use simultaneously the HD coils describe above. It was proposed to reduce the local heat flux to ~1/10 by having a sweeping distance of ~800 mm in the poloidal direction. This should be, however, considered to be the maximum case. If the width is 240 mm, the effective heat flux could be ~1/3 and the amplitude of the HD coils would be ~1/4 of the maximum case. For the RMP and HD coils, we note that a similar HTS STARS conductor can be applied. Like the main helical coils, the STARS conductor can be wound with joint winding method. In the present analysis, the RMP coils have oval shapes. We will employ more realistic shapes of the RMP coils in our future studies to accommodate the port structures.

Thus, in conclusion, for the peak heat flux reduction, the above two methods were thought to have only some limited solution.

On the other hand, it is noted that there could be almost no change in the alpha particle confinement by including perturbations in the ergodic field regions especially using the HD coils, because the magnetic surfaces are not changed inside the LCFS. For the RMP coils, the magnetic surfaces are slightly altered. However, even in this case, the core region is almost the same and thus there must be no practical change in the energetic particle confinement. Detailed calculations will be performed and reported in our future studies.

4.3 Discussion on the liquid divertor option

To accommodate the possible large peak heat flux, which is discussed above, it was proposed to use a liquid divertor option instead of the conventional solid divertor. The liquid divertor system is called REVOLVER-D and the details are discussed in [55]. As is described above, by considering the feature that the divertor footprints are concentrated on the inboard side of the torus with the inward-shifted magnetic configuration of FFHR-d1A, it is proposed to install ten units of molten tin (Sn) shower jets (vertical falls) on the inboard side of the torus to intersect the ergodic layers. This works as an ergodic divertor/limiter. For the liquid metal material, tin is selected because of its low melting temperature, low vapor pressure, low material cost, and high safety. It is proposed that the vertical flow of tin jets could be stabilized using metal chains imbedded. Neutral particles are expected to be efficiently evacuated through the gaps between liquid metal showers.

The first priority of using liquid divertor is found in its capability to accommodate high heat flux of ~100 MW/m^2 or even higher. At the same time, other crucial features of the liquid divertor are recognized in its high maintainability and low waste production. We note that one of the difficult issues related to the helical divertor, in addition to the non-uniform flux problem, is the maintenance scheme. This is discussed in the later section. Compared to this situation, the maintenance work of a liquid divertor system would become much easier [55]. Moreover, the waste production would become another significant issue for the helical divertor, whereas the problem would be much reduced for the liquid divertor system.

Though it seems that the liquid divertor option is attractive, we have to note that there still remain a number of technological issues to be solved in order to actually employ this option. In fact, the basic research and development of REVOLVER-D system has just begun. The MHD effect is considered to be a serious problem for this type of open liquid divertor, as discussed in [56], even though the helical plasma is free from significant transients, such as disruptions. This problem is now being investigated fully and the necessary modification is being implemented, which will be reported elsewhere. Moreover, even if the liquid divertor can be actually employed in our future design, and the full-helical divertor becomes less necessary, we cannot completely remove them. This is because of the fact that not all the flux can be handled completely only by the liquid divertor and some portion of the flux would reach the helical divertor. Even if the remaining flux is ~5%, this corresponds to ~30 MW of power handling.

4.4 Reexamination of the helical divertor

We thus examine the feasibility of the helical divertor again for the FFHR design. On this occasion, we here introduce a random walk process in the numerical calculation of magnetic field-line tracing in order to crudely simulate the collision processes in the plasma, which may contribute in flattening the peak heat flux. In the present calculation, the diffusion coefficient is assumed to be ~0.5 m^2/s [57, 58], and this crudely gives typically a deviation of ~6 mm for a path length of 1 m along a field-line. At the same time, the effective width of the strike points is also evaluated, rather than simply assuming to be 80 mm all along. The results are shown in Fig. 10 for the cases both with and without including the random walk process. It is found that the effective width of strike points is larger than our original estimation of 80 mm, especially at the peak heat flux location. This seems primarily so even in the case of not including the random walk process. In fact, the effective width is estimated to be almost ~200 mm. Here, the width is estimated by measuring the distance from the helical coil center to the footprint as shown by Z_{div} in Fig. 3. We note that this Z_{div} rotates along with the helical coil. By taking account of the random walk process, it is found in Fig. 11(a) that the peak flux is lowered and its toroidal location is shifted. Considering this fact that the effective width of strike points become wider, the peak heat flux is supposed to become much lower than the previous estimation of ~100 MW/m^2. In the case that the random walk process is included, the peak flux of divertor strike points is even lowered. We note that in this case, there is a possibility that the peak heat flux almost disappears and the heat flux all over the helical divertors could be at a tolerable level with the presently developed tungsten divertor with copper-alloy cooling pipes. It is also noted again that this is for the case of 3 GW fusion power production (600 MW coming to the divertor) and no radiation dispersion is assumed.

A similar calculation is performed for the FFHR-d1C configuration as shown in Fig. 11(b). In this case, it is considered that the strike points are concentrated on the outboard side of the torus, due to the slightly outward shifted magnetic configuration, which corresponds to the case of R = 3.75 m in LHD. In this case, as is seen in Fig. 2 for FFHR-d1A, the effective width of divertor strike points becomes narrow, and there is a concern that the heat flux would become higher than the case for FFHR-d1A. However, we also note that the power handling on the outboard side is supposed to be generally easier than is the case on the inboard side of the torus. Similar calculations are done by including the RMP coils, and the results are shown in Fig. 12 both for the FFHR-d1A and d1C-SO configurations. In our future studies, numerical simulations using the EMC3-EIRENE code [59] will be performed for the FFHR reactor design so that the heat flux on divertor plates could be more precisely evaluated by taking account of the parallel and perpendicular diffusion processes in the edge plasma.

Figure 13 shows an illustration of the layout of the helical divertor. The divertor plates and pipes could be replaced by units using ports. The three-dimensional maintenance scheme for the full-helical divertor should be investigated in our future work.

5. Aquarium method for the maintenance of the helically-segmented breeder blanket and the helical divertor

For the tritium breeding blanket of FFHR, we have chosen the liquid blanket option with molten salt FLiNaBe (melting point: 580 K) from the perspective of passive safety [60]. To increase the hydrogen solubility, an innovative idea to include powders of titanium [61] was proposed. An increase of hydrogen solubility over five orders of magnitudes has been confirmed in an experiment [62], which makes tritium permeation barrier less necessary for the coating on the walls of cooling pipes. The "Oroshhi-2" facility was constructed as a platform for international collaboration, having a twin-loop for testing both molten-salt (FLiNaK) and liquid metal (LiPb) under the perpendicular magnetic field of 3 T [62]. For the structural material of blankets, a dissimilar bonding technique has been developed to join the vanadium alloy, NIFS HEAT2, and a nickel alloy. Figure 14 shows an illustration of the blanket system with helically-segmented parts.

For the engineering design of the helical reactor, the maintenance scheme of the breeder blankets as well as the helical divertor is a critical issue associated with the 3D complicated structure. It has been confirmed that large port areas can be situated between the helical coils, and the electromagnetic forces and stresses in the coil supporting structures tolerate this condition [63]. This is useful from the viewpoint of conducting the maintenance work. In this respect, the "screw coaster" method was proposed for FFHR2m1 [63], in which remote handling tools go along the helical path (like a "helically-moving roller coaster") to replace the blanket components. However, the important issue is how we can install and operate remote handling tools inside the vacuum vessel where the gamma ray environment may reach up to an extremely high dose rate of ~10 kSv/h, which is much more intense than the situation in ITER. The lifetime of a robotic arm would become very short in such an environment. Furthermore, it is necessary that the divertors should be maintained separately from the blankets. In this respect, the divertor is provided by cartridges in tokamaks. For the helical divertor in the helical fusion reactor, a cartridge type helical divertor is not possible because of the three-dimensionally continuous nature. In this respect, a completely new proposal is to use the liquid divertor, as is described in the previous section, to provide better maintenance capability. On the other hand, for the blanket, a cartridge type may be possible. A toroidally segmented method, T-SHELL, was first proposed for this purpose, which divides the blanket segments at every 3° in the toroidal angle [64]. This is similar to the vertical maintenance scheme for tokamak reactors. For the helical reactor, it is necessary to move the segments further in the toroidal and poloidal directions than is the situation in tokamaks, which may give additional difficulties. Thus, a further segmentation is proposed, which is called the CARDISTRY blanket [65]. It is noted that this is a similar idea to the horizontal maintenance scheme for tokamaks. Although this seems to be a revolutionary idea, we must note that there would be many engineering issues to be solved in order to realize this idea. Moreover, the liquid divertor is also combined fully with this idea [65]. The details regarding the problem of this method are described elsewhere.

In this paper, a completely different idea is proposed, which provides a practical solution to use the helical divertor and helically-segmented blanket with a remote handling system for maintenance works. The idea is to fill the vacuum vessel with water after the termination of

fusion power generation before starting the maintenance work. The dose rate of gamma rays could become three orders of magnitude lower by having 1.5-m-thick water. This should prolong the lifetime of robotic arms significantly. Further shielding can be provided to protect the electronic devices equipped on the robotic arms. This method is called the "aquarium method." Figure 15 shows an illustrated image of this method. The aquarium method is considered to be useful also for significantly reducing the overall gamma ray radiation level to the environment outside the reactor when the first port is opened. The procedure for the "Aquarium Method" is described as follows:

After the termination of the fusion power generation, cooling of the blanket is continued by keeping the molten-salt. Before reaching the melting temperature during the cooling, the molten-salt is drained from the breeding blankets. Then, the cooling is continued by switching to helium gas. We must wait until the temperature becomes sufficiently low to be close to ~100 centigrade. We must be careful that the temperature of tungsten should be lower than 300 centigrade to avoid oxidization. Then, a water shower at a temperature of ~100 centigrade is sprayed toward the first wall. We note that using water is effective also to remove tritium from the first wall surface [66]. When the vaporization of water becomes weak due to the decrease of the temperature, the entire amount of water is finally poured into the vacuum vessel gradually. When the water is filled to the top, the upper ports are opened and robotic arms are installed. The blanket parts and pipes are disconnected and dismounted using robotic arms. The divertor tiles and pipes are also disconnected and dismounted. These parts are collected at the upper port areas on the water surface. Then, the parts are installed into casks and transported to a storage room by moving in the corridor located above the torus. The laser welding technique underwater is necessary to dismount the blanket and divertor parts. We note that this technique has already been practically established for application to fission reactors [67].

We also note that a similar (but different) idea using water in a fusion reactor was proposed in the 1980's [68]. In that proposal, the water was supposed to be filled outside the vacuum vessel. In the present proposal, the water should fill the inside of the vacuum vessel. Thus its effect especially on the RAFM and tungsten, with respect to high-temperature plasma production, should be carefully examined. With the exception of this, the basic idea could be regarded as similar to the case of fission reactors in which vessels are filled with water also during the maintenance work. Handling and recovery of tritium from >10,000 tons of water is another crucial issue.

6. Conclusions

The conceptual design of the LHD-type helical fusion reactor FFHR-d1 has been steadfastly progressing. The present standard design is FFHR-d1A as the engineering basis, and a higher magnetic field version FFHR-d1B is also proposed. In order to attain a higher Q-value with lower magnetic field (lower cost), a configuration optimization is carried out as FFHR-d1C. There is a possibility that a slightly modified trajectory of the continuously-wound helical coils gives a better tradeoff between the confinement and the MHD stability of the core plasma. The helical divertors are better protected by blankets from the incident neutrons emitted from the core plasma so that a copper-alloy can be applied to accommodate high heat flux.

The engineering design studies of FFHR-d1 are focused on the ideas for overcoming the complexity associated with the three-dimensional structures for the superconducting helical coils, helical divertors, and helically-segmented breeder blankets.

The magnet system employs the 100-kA-class HTS STARS conductor having simple stacking of REBCO tapes and an internal electrical insulation. The joint-winding of the helical coils using segmented conductors with mechanical lap joint is expected to be completed in <3 years, if the fabrication of one joint is completed in one day.

The helical divertor is reexamined. Due to the large toroidal non-uniformity of the divertor strike points observed in the field-line tracing, it was considered that a large peak heat flux of up to ~100 MW/m^2 would come to the inboard side of the torus for a 3 GW fusion power generation. In this case, the radiation dispersion would be inevitable. However, there is no guarantee that a detachment could be realized continuously. To mitigate the non-uniform distribution of the divertor flux, two proposals were made previously using RMP coils and HD coils. However, both types of coils were found to have only limited effects. In this respect, a liquid divertor system could be a new option to deal with a large heat flux, though there are a number of engineering issues to be solved. By examining the effective width of the strike points and by including random walk processes to simulate collisions in the plasma, it is recently recognized that the strike points could become more flattened. Thus, there is a possibility that the heat flux would become at a technically tolerable level with the presently developed tungsten tiles with copper-alloy cooling pipes. We note that no radiation dispersion is assumed in this estimation.

The remaining critical issue for the helical divertor is the maintenance, similar to the helically-segmented breeder blankets. The three-dimensional maintenance procedure using remote handling tools would suffer from the intense gamma ray environment of up to ~10 kSv/h. This situation would be eased using the “Aquarium method,” by filling the vacuum vessel with water. The detailed investigation of this method will be performed in our future studies. There also remains another issue that a large amount of waste is accumulated with the helical divertor during maintenance works in comparison to the situation of using the liquid divertor system. We must find a plausible method in our future study to reduce the amount of materials required for the helical divertor.

Acknowledgments

The authors thank the members of the Fusion Engineering Research Project at NIFS, especially, T. Mito, S. Hamaguchi, S. Imagawa, K. Takahata, A. Iwamoto, T. Obana, H. Chikaraishi, N. Ashikawa, M. Tokitani, G. Kawamura, Y. Hamaji, R. Sakamoto, and S. Masuzaki for fruitful discussions. Special thanks are given to T. Muroga and H. Yamada. One of the authors (N. Y.) is grateful for the continuous discussion and encouragement given by A. Komori regarding the feasibility of the helical divertor. The optimized configuration provided by S. Okamura is highly appreciated. The NITA coil configuration was proposed by the late T. Watanabe, who made tremendous contributions to the FFHR design activities. The design of the helical divertor and the helically-segmented blanket made by S. Kinoshita at Hitachi Ltd. are greatly acknowledged. This work was supported in part by the Japan Society for the Promotion of Science (JSPS) Grant-in-Aid for Scientific Research (S) under Grant 26220913.

References

[1] A. Sagara, et al., “Review of stellarator/heliotron design issues towards MFE DEMO”, Fusion Engineering and Design **85** (2010) 1336.

[2] A. Sagara, et al., “Helical reactor design FFHR-d1 and c1 for steady-state DEMO”, Fusion Engineering and Design **89** (2014) 2114.

[3] A. Sagara, et al., “Two conceptual designs of helical fusion reactor FFHR-d1A based on ITER technologies and challenging ideas”, Nuclear Fusion **57** (2017) 086046.

[4] A. Sagara, et al., “Design studies of helical-type fusion reactor FFHR”, Fusion Engineering and Design **41** (1998) 349.

[5] L.A. El-Guebaly, “Fifty years of magnetic fusion research (1958–2008): brief historical overview and discussion of future trends” Energies **3** (2010) 1067.

[6] A. Komori, et al., “Development of net-current free heliotron plasmas in the Large Helical Device”, Nuclear Fusion **49** (2009) 104015.

[7] Y. Takeiri, “Prospect towards steady-state helical fusion reactor based on progress of LHD project entering the deuterium experiment phase”, IEEE Transactions on Plasma Science **99** (2017) 1.

[8] M. Osakabe, “Preparation and commissioning for the LHD deuterium experiment”, IEEE Transactions on Plasma Science **99** (2018) 1.

[9] A. H. Boozer, “What is a stellarator?”, Physics of Plasmas **5** (1998) 1647.

[10] C. D. Beidler, “Stellarator fusion reactors - an overview”, J. Plasma Fusion Res. SERIES **5** (2002) 149.

[11] F. Warmer, et al., “From W7-X to a HELIAS fusion power plant: motivation and options for an intermediate-step burning-plasma Stellarator”, Plasma Physics and Controlled Fusion **58** (2016) 074006.

[12] F. Najmabadi, et al., “The ARIES-CS compact stellarator fusion power plant”, Fusion Science and Technology **54** (2008) 655.

[13] H. Tamura, et al., “Design of structural components for the helical reactor FFHR-d1A”, Fusion Engineering and Design **89** (2014) 2336.

[14] H. Tamura, et al., “Design modification of structural components for the helical fusion reactor FFHR-d1 with challenging options”, Fusion Engineering and Design **124** (2017) 605.

[15] Y. Chida, et al., “Validation of welding technology for ITER TF coil structures”, Fusion Engineering and Design **86** (2011) 2900.

[16] T. Goto, et al., “Design window analysis for the helical DEMO reactor FFHR-d1”, Plasma Fusion Res. **7** (2012) 2405084.

[17] J. Miyazawa, et al, “Direct extrapolation of radial profile data to a self-ignited fusion reactor based on the gyro-Bohm model”, Fusion Eng. Des. **86** (2011) 2879.

[18] T. Goto, et al., “Development of a real-time simulation tool towards self-consistent scenario of plasma start-up and sustainment on helical fusion reactor FFHR-d1”, Nuclear Fusion **57** (2017) 066011.

[19] S. Okamura, “Configuration optimization of planar-axis stellarator with minimum number of Fourier modes of boundary shape”, Plasma Phys. Control. Fusion **55** (2013) 032002.

[20] S. Okamura, “Configuration Optimization of a Planar-Axis Stellarator with a Reduced Shafranov Shift”, Plasma and Fusion Research **8** (2013) 2402029.

[21] N. Yanagi, et al., “NITA coil — Innovation for enlarging the blanket space in the helical fusion reactor”, Plasma and Fusion Research **11** (2016) 2405034.

[22] R. Kanno, et al., “Formation and healing of n=1 magnetic islands in LHD equilibrium”, Nuclear Fusion **45** (2005) 588.

[23] Y. Masaoka and S. Murakami, “Study of α-particle confinement in an LHD-type heliotron reactor”, Nuclear Fusion **53** (2013) 093030.

[24] R. Seki, et al., “Monte Carlo study based on a real coordinate system for tangentially injected high-energy particles in the Large Helical Device”, Plasma and Fusion Research **5** (2010) 027.

[25] G. Bansal, et al., “High-temperature superconducting coil option for the LHD-type fusion energy reactor FFHR”, Plasma and Fusion Research **3** (2008) S1049.

[26] N. Yanagi, et al., “Design progress on the high-temperature superconducting coil option for the heliotron-type fusion energy reactor FFHR”, Fusion Science and Technology **60** (2011) 648.

[27] N. Yanagi, et al., “Feasibility of HTS magnet option for fusion reactors”, Plasma and Fusion Research **9** (2014) 1405013.

[28] N. Yanagi, et al., “Design and development of high-temperature superconducting magnet system with joint-winding for the helical fusion reactor”, Nuclear Fusion **55** (2015) 053021.

[29] S. Imagawa, et al., “Concept of magnet systems for LHD-type reactor”, Nuclear Fusion **49** (2009) 075017.

[30] A. Sagara, et al., “Optimization activities on design studies of LHD-type reactor FFHR”, Fusion Engineering and Design **83** (2008) 1690.

[31] Y. Terazaki, et al., “Critical current measurement of 30 kA-class HTS conductor samples”, IEEE Trans. Appl. Supercond. **24** (2014) 4801305.

[32] Y. Terazaki, et al., “Measurement and analysis of critical current of 100-kA class simply-stacked HTS conductors”, IEEE Trans. Appl. Supercond. **25** (2015) 4602905.

[33] S. Ito, et al., “Bridge-type mechanical lap joint of a 100 kA-class HTS conductor having stacks of GdBCO tapes”, Plasma and Fusion Research **9** (2014) 3405086.

[34] S. Ito, et al., “Mechanical and electrical characteristics of a bridge-type mechanical lap joint of HTS STARS conductors”, IEEE Trans. Appl. Supercond. **26** (2016) 4201510.

[35] K. Uo, et al., “Contact resistance of demountable multi-pin joint for superconducting helical coil”, Proceedings of 14th Symposium on Fusion Technology (1986) 1727.

[36] H. Hashizume, et al., “Proposal of mechanically jointed superconducting magnet using high critical temperature superconductors”, Fusion Engineering and Design **63** (2002) 449.

[37] H. Tamura, et al., “Multiscale stress analysis and 3D fitting structure of superconducting coils for the helical fusion reactor”, IEEE Transactions on Applied Superconductivity **26** (2016) 4202405.

[38] T. Nishio, et al., “Reducing joint resistance by heat treatment during fabrication of a mechanical joint of high-temperature superconducting conductors”, IEEE Transactions on Applied Superconductivity **26** (2016) 4800505.

[39] N. Yanagi, et al., “Magnet design with 100-kA HTS STARS conductors for the helical fusion reactor”, Cryogenics **80** (2016) 243.

[40] S. Hahn, et al., “HTS pancake coils without turn-to-turn insulation”, IEEE Transactions on Applied Superconductivity **21** (2011) 1592.

[41] S. Ito, et al., “Fundamental investigation on tensile characteristics of a mechanical lap joint of REBCO tapes”, IEEE Transactions on Applied Superconductivity **25** (2015) 4201205.

[42] S. Ito, et al., “Advanced high-temperature superconducting magnet for fusion reactors: Segment fabrication and joint technique”, Fusion Engineering and Design (2018).

[43] K. Uo, “The confinement of plasma by the heliotron magnetic field”, Journal of the Physical Society of Japan **16** (1961) 1380.

[44] C. Gourdon, et al., “The torsatron without toroidal field coils as a solution of the divertor problem”, Nuclear Fusion **11** (1971) 161.

[45] H. Nakashima, et al., “Neutron streaming analysis for helical geometry system, Heliotron-H fusion power reactor”, Journal of Nuclear Science and Technology **23** (1986) 287.

[46] T. Tanaka, et al., “Neutronics investigations for helical demo reactor FFHR-d1”, Plasma and Fusion Research **7** (2012) 2405132.

[47] H. Tamura, et al., “Novel divertor design to mitigate neutron irradiation in the helical reactor FFHR-d1”, Fusion Engineering and Design **98-99** (2015) 1629.

[48] H. Tamura, et al., “Radial-build design and support system for the helical DEMO reactor FFHR-d1”, Fusion Engineering and Design **88** (2013) 2033.

[49] Masuzaki, et al., “The divertor plasma characteristics in the Large Helical Device”, Nuclear Fusion **42** (2002) 750.

[50] S. Masuzaki, et al., “Edge plasma transport in the helical divertor configuration in LHD”, Contributions to Plasma Physics **50** (2010) 629.

[51] M. Kobayashi, et al., “Control of 3D edge radiation structure with resonant magnetic perturbation fields applied to the stochastic layer and stabilization of radiative divertor plasma in LHD”, Nuclear Fusion **53** (2013) 093032.

[52] N. Yanagi, et al., “Heat flux reduction by helical divertor coils in the heliotron fusion energy reactor”, Nuclear Fusion **51** (2011) 103017.

[53] Y. Nakamura, et al., “Impact of real-time magnetic axis sweeping on steady state divertor operation in LHD”, Nuclear Fusion **46** (2006) 714.

[54] N. Yanagi, et al., “Divertor heat flux reduction by resonant magnetic perturbations in the LHD-type helical demo reactor”, 24th IAEA Fusion Energy Conference, San Diego (2012) FTP/P7-37.

[55] J. Miyazawa, et al., “Conceptual design of a liquid metal limiter/divertor system for the FFHR-d1”, Fusion Engineering and Design **125** (2017) 227.

[56] F. L Tabarés, “Present status of liquid metal research for a fusion reactor”, Plasma Physics and Controlled Fusion **58** (2016) 014014.

[57] T. Morisaki, et al., “Review of divertor studies in LHD”, Plasma Science and Technology **8** (2006) 14.

[58] N. Ohyabu, et al., “The Large Helical Device (LHD) helical divertor”, Nuclear Fusion **34** (1994) 387.

[59] G. Kawamura, et al., “First EMC3-EIRENE simulations with divertor legs of LHD in realistic device geometry”, Contributions to Plasma Physics **54** (2014) 437.

[60] A. Sagara, et al., “Blanket and divertor design for force free helical reactor (FFHR)”, Fusion Eng. Des. **29** (1995) 51.

[61] J. Yagi, et al., “Hydrogen solubility in FLiNaK mixed with titanium powder”, Fusion Engineering and Design **98–99** (2015) 1907.

[62] A. Sagara, et al., “First operation of the Flinak/LiPb twin loop OROSH2I-2 with a 3T SC magnet for R&D of liquid blanket for fusion reactor”, Fusion Science and Technology **68** (2015) 303.

[63] A. Sagara, et al., “Conceptual design activities and key issues on LHD-type reactor FFHR”, Fusion Eng. Des. **81** (2006) 2703.

[64] T. Goto, et al., “Proposal for the method of maintaining breeder blankets in the LHD-type helical fusion reactor FFHR”, Plasma and Fusion Research **11** (2016) 2405047.

[65] J. Miyazawa, et al., “Cartridge-type helical blankets aiming at easy construction and maintenance for the FFHR-d1”, Plasma and Fusion Research **12** (2017) 1405017.

[66] W. T. Shmayda, et al., “Dependence of tritium release from stainless steel on temperature and water vapor”, Fusion Science and Technology **68** (2015) 1.

[67] M. Yoda, et al., “Underwater laser beam welding for nuclear reactors”, Proceedings on 2012 20th International Conference on Nuclear Engineering and the ASME 2012 Power Conference, Anaheim, California, USA, July 30-August 3, 2012 (2012) 191.

[68] K. Sako, et al., “Design study of swimming pool type tokamak reactor (SPTR)”, Journal of Nuclear Science and Technology **19** (1982) 491.

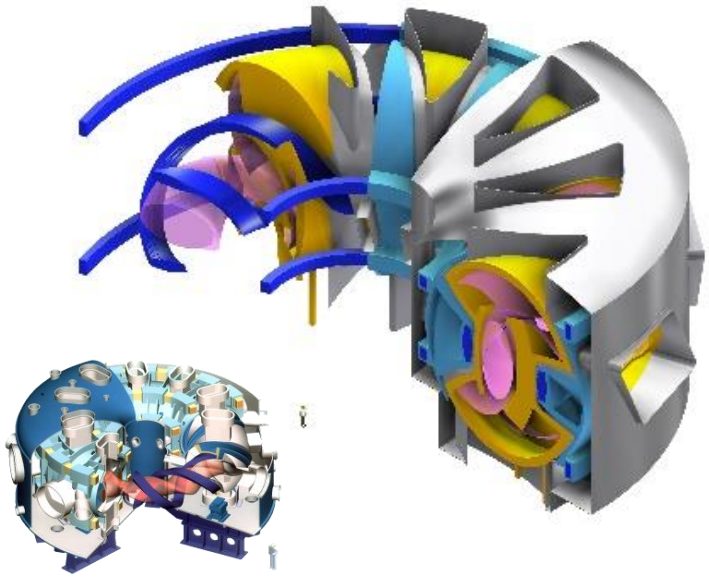

Fig. 1. Schematic comparison between LHD (left) and FFHR-d1 (right).

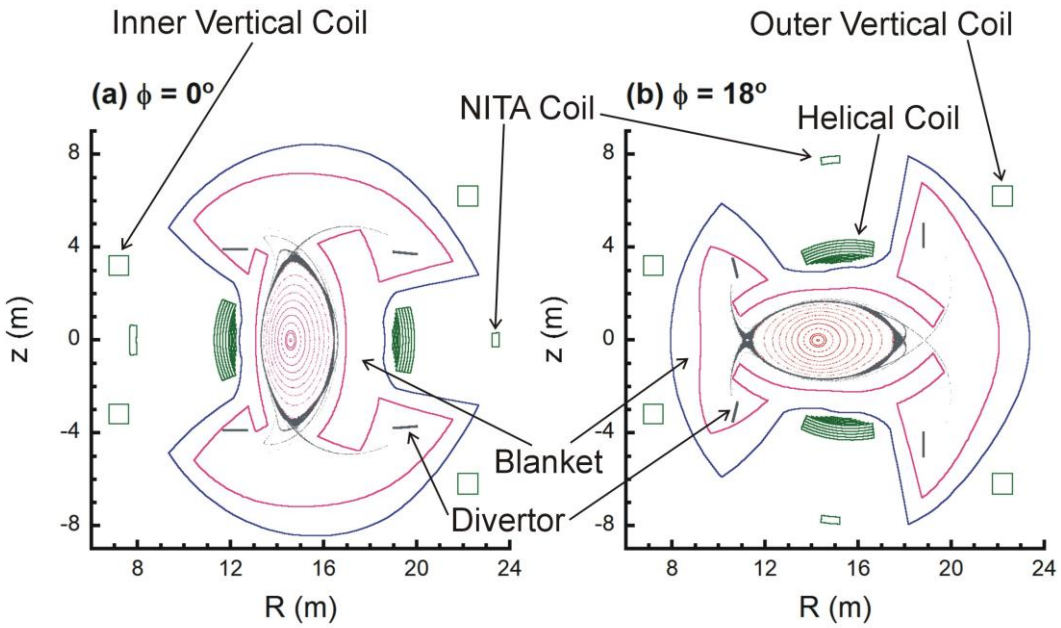

Fig. 2. Vacuum magnetic surfaces of FFHR-d1 with NITA coils at toroidal angles (a) $\phi = 0°$ and (b) 18°. The toroidal angle is defined in Fig. 3.

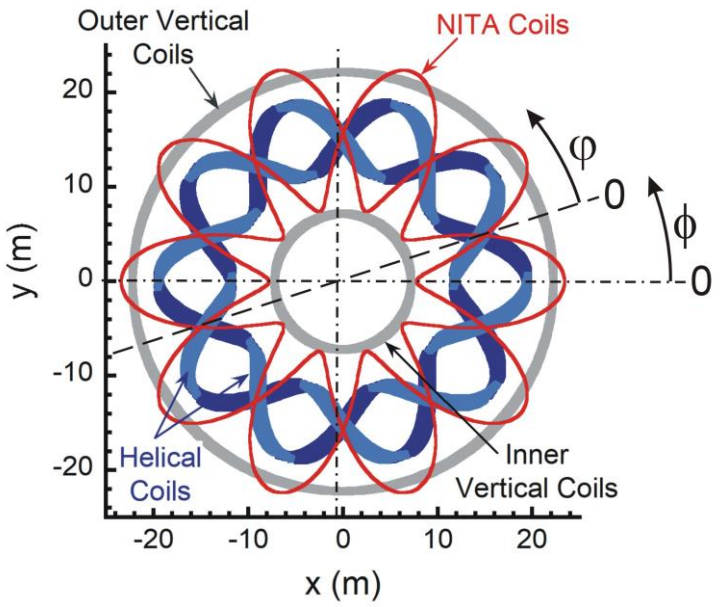

Fig. 3. A plan view of the coil system of FFHR-d1. The definitions of the two toroidal angles ϕ and φ are indicated. The NITA coils are wound outside the main helical coils.

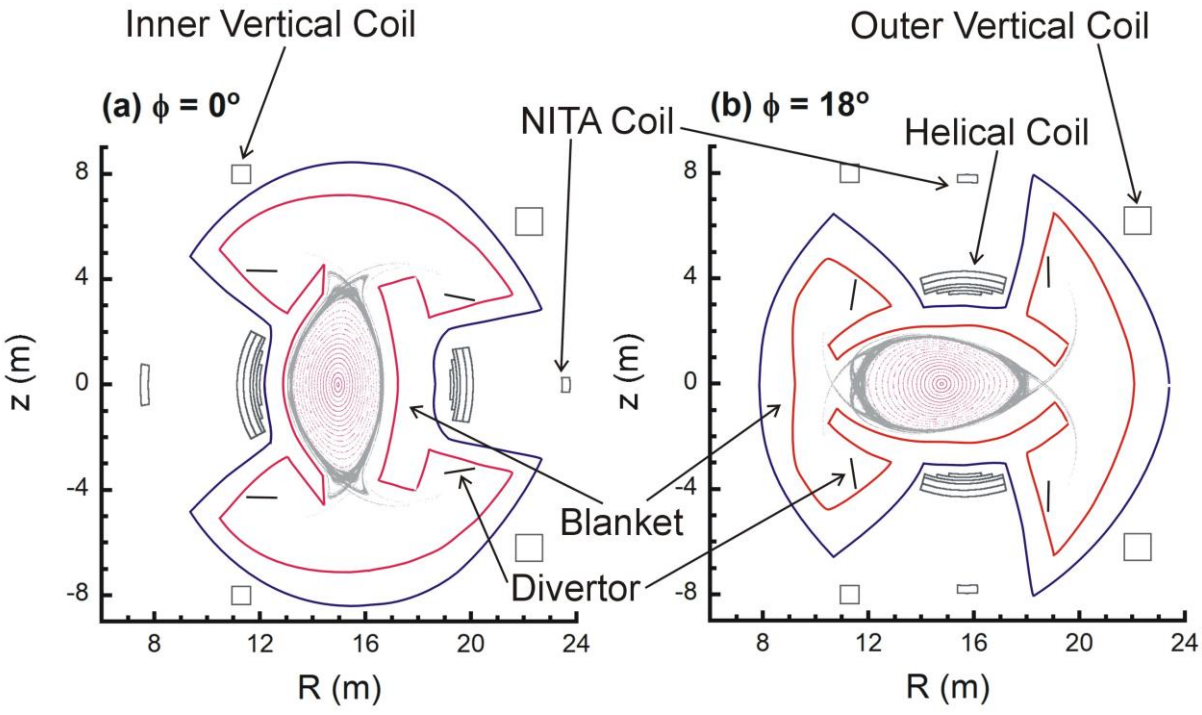

Fig. 4. Vacuum magnetic surfaces of FFHR-d1C-SO with NITA coils at toroidal angles (a) ϕ = 0° and (b) 18°.

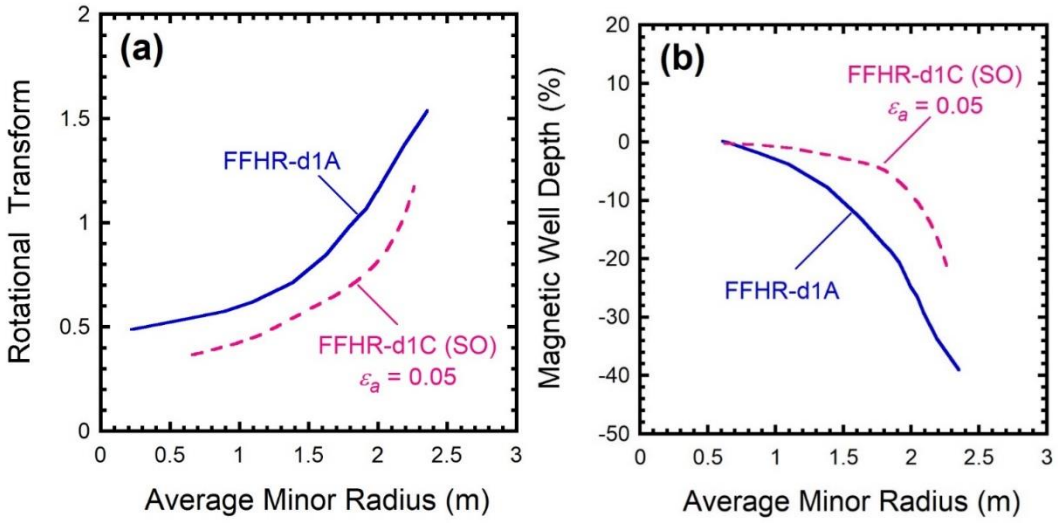

Fig. 5. Comparison of the rotational transform and magnetic well as a function of the average minor radius between FFHR-d1A and FFHR-d1C-SO in the vacuum condition.

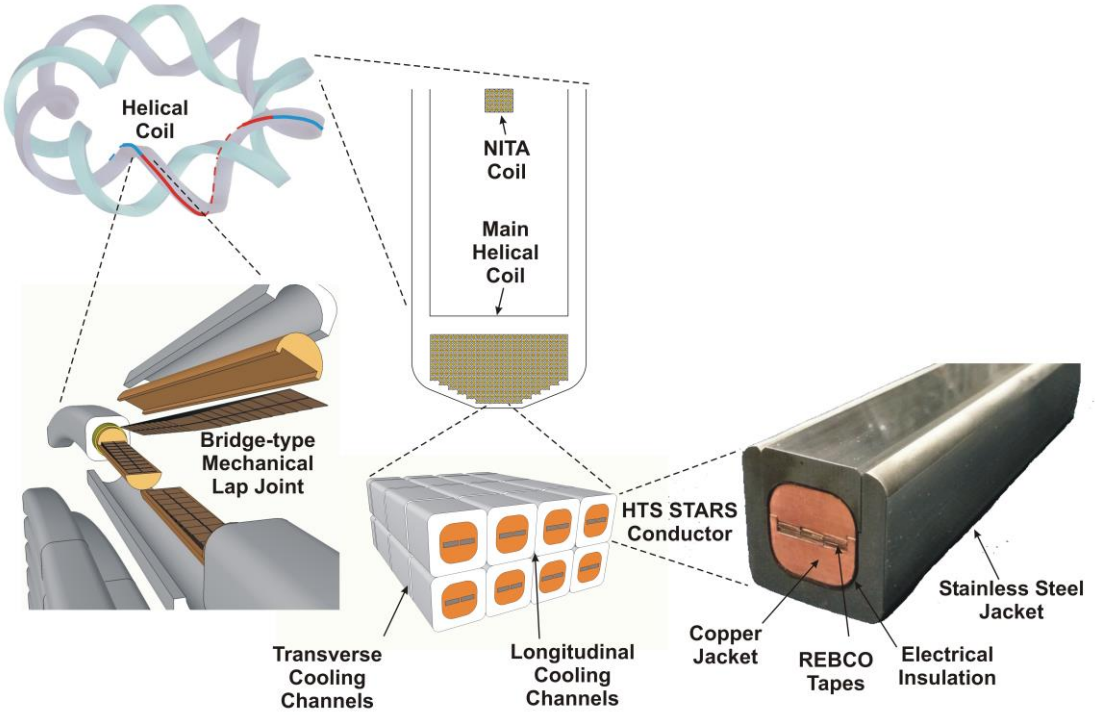

Fig. 6. Schematic illustration of the FFHR-d1 helical coils with HTS STARS conductors. The "joint-winding" method is indicated with one-helical-pitch conductor segments. The cross-sectional view of the main helical coil (winding package) and a sub-helical coil (NITA coil) is also shown. A photograph of a mockup of the STARS conductor is also shown.

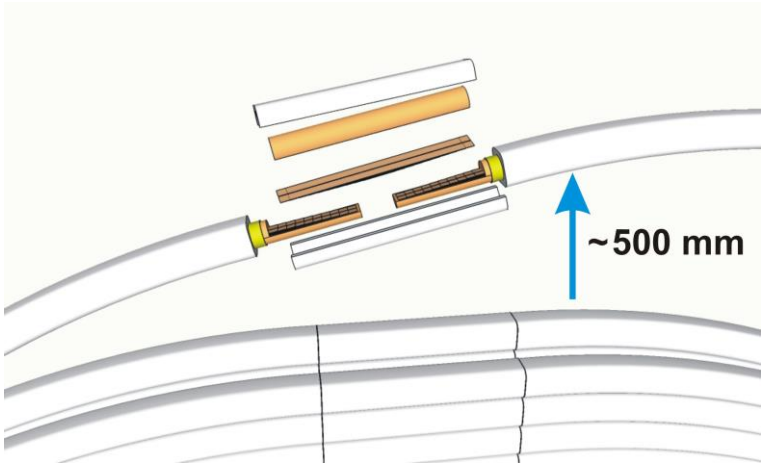

Fig. 7. A close-up view of the joint section in the FFHR-d1 helical coils. The joint section is raised at ~500 mm above the final position.

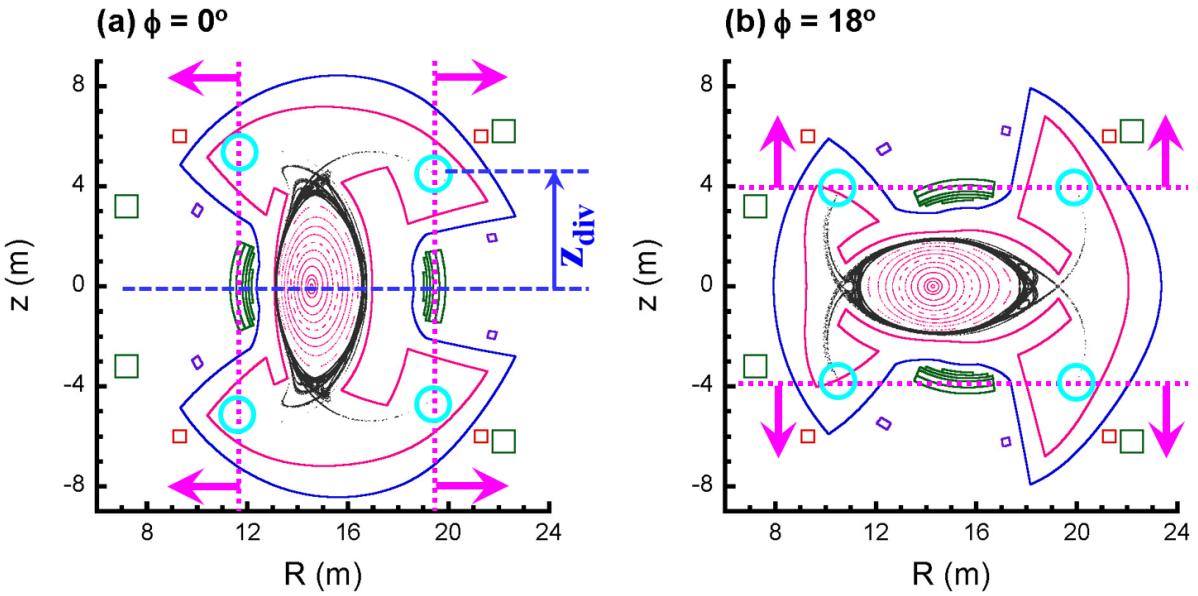

Fig. 8. Vacuum magnetic surfaces of FFHR-d1A at toroidal angles (a) $\phi = 0°$ and (b) 18°. The toroidal angle is defined in Fig. 3. The dashed lines indicate planes with the minor radius of the helical coils that rotate in the toroidal direction along with the helical coils. When the magnetic field-line crosses these planes (as indicated by the arrows), the divertor footprints are collected. The distance from the helical coil center to this footprint is measured as Z_{div},. Note that Z_{div} is defined in each toroidal angle rotating along with the helical coil.

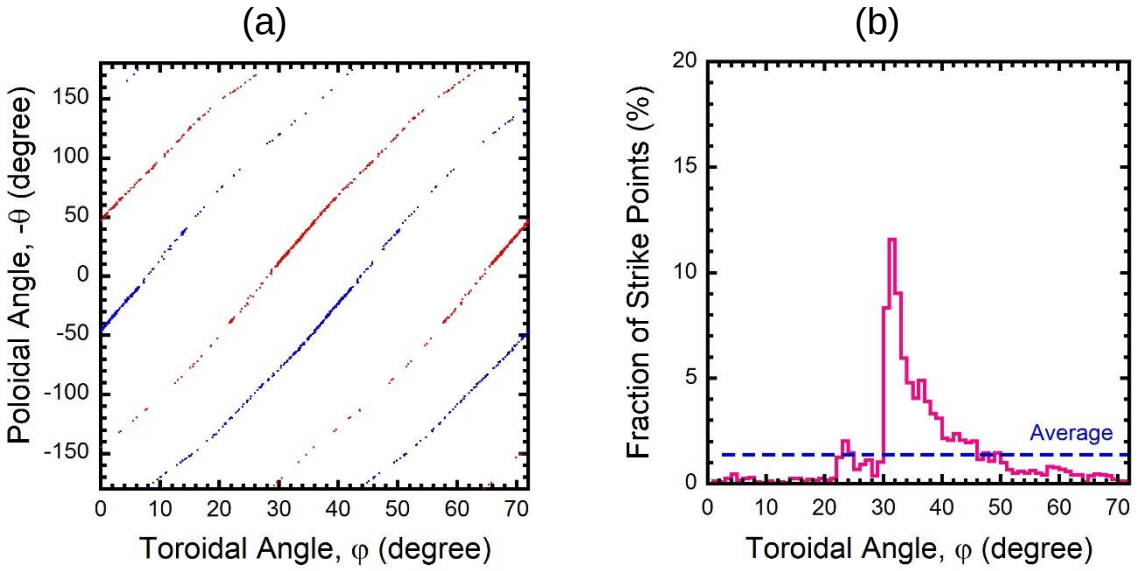

Fig. 9. (a) Footprints of magnetic field-lines coming to the divertor regions of the FFHR-d1 configuration on the toroidal and poloidal angle plane. The red and blue points correspond to footprints coming from two divertor legs having the positive and the negative toroidal directions of magnetic field, respectively. (b) Histogram compiled for one of the footprints (in the positive direction of the toroidal angle) with a 1° pitch.

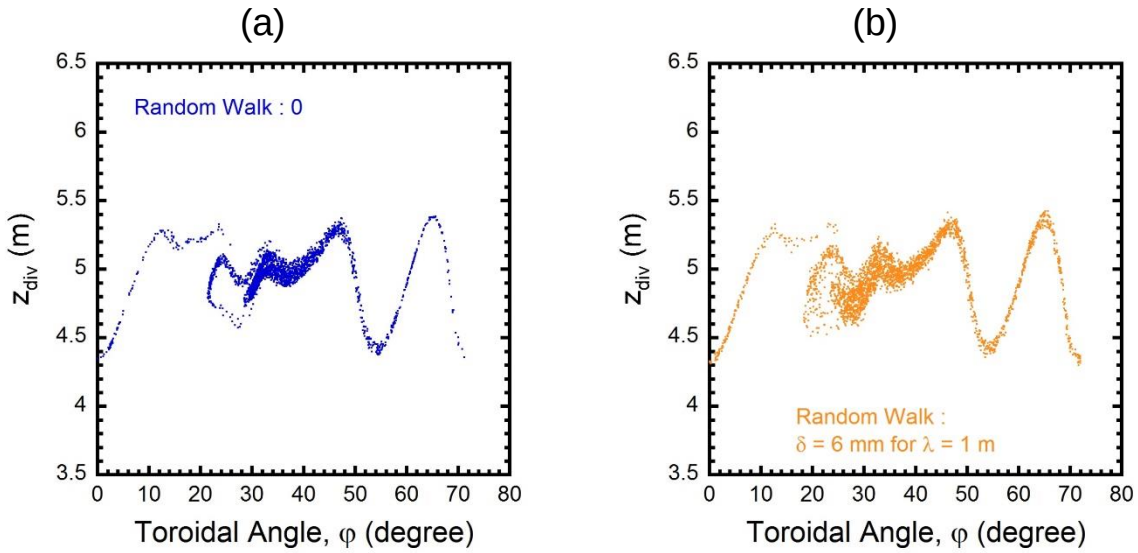

Fig. 10. Plot of the distance from the helical coil center to the footprint, Z_{div}, measured in Fig. 3 for FFHR-d1A as a function of the toroidal angle for the two cases (a) without a random walk process in the field-line tracing and (b) with this process.

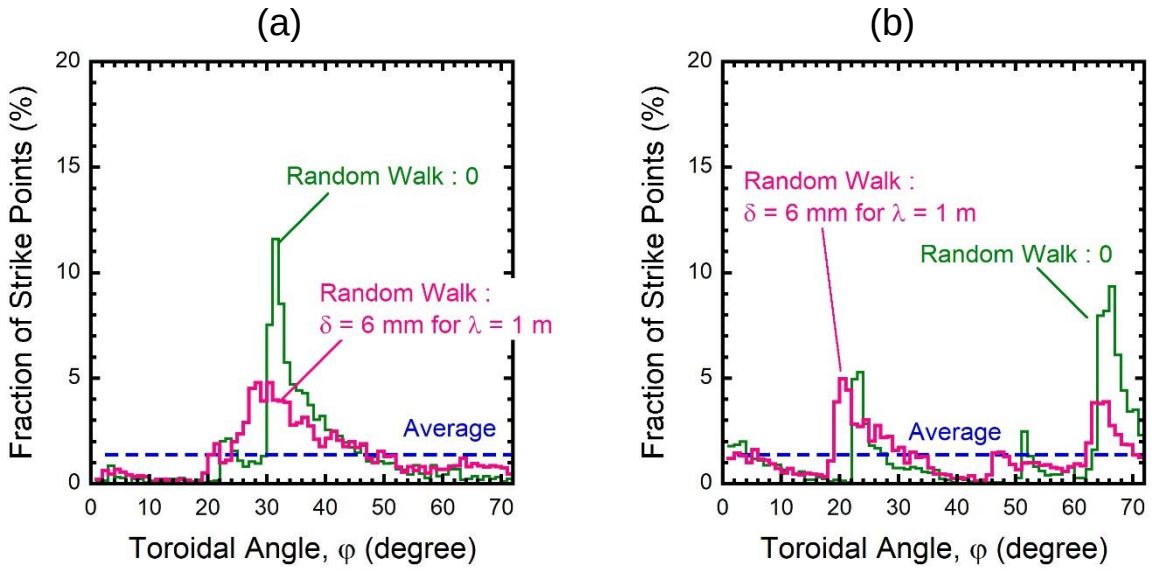

Fig. 11. (a) Fraction of the number of strike points of magnetic field-lines coming to the divertor regions for the FFHR-d1A configuration, plotted as a function of the toroidal angle with and without including the random walk process. (b) The same calculation for the FFHR-d1C-SO configuration. Calculations are performed for the total of 5184 starting points of magnetic field-line tracing.

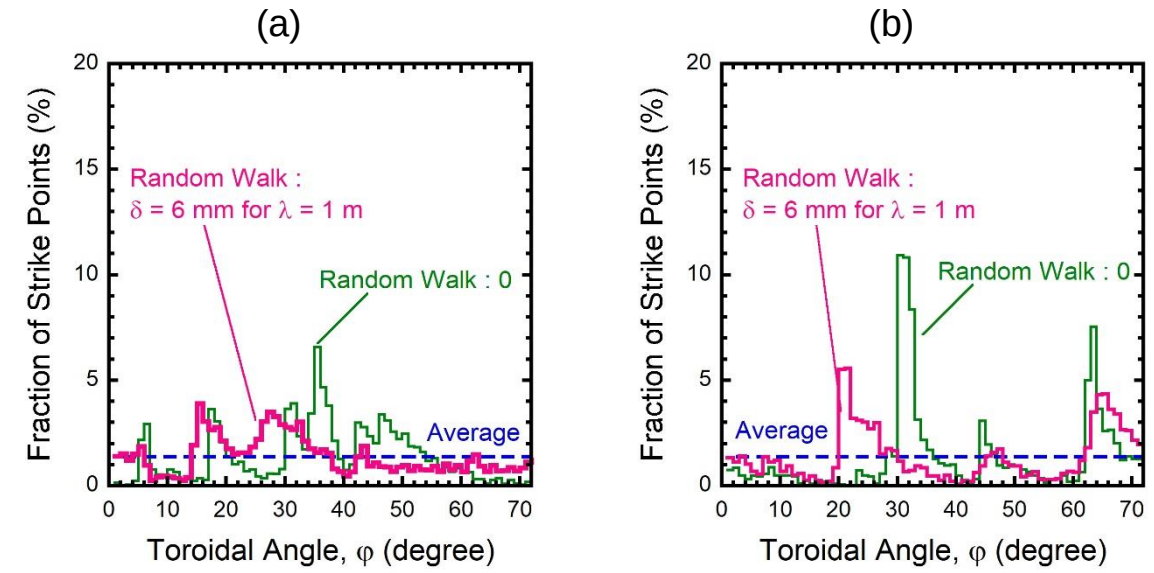

Fig. 12. (a) Fraction of the number of strike points of magnetic field-lines coming to the divertor regions for the FFHR-d1A configuration including the RMP coils with each 6 MA current, plotted as a function of the toroidal angle with and without taking the random walk process. (b) The same calculation for the FFHR-d1C-SO configuration, also with the RMP coil current of each 6 MA. Calculations are performed for the total of 5184 starting points of magnetic field-line tracing.

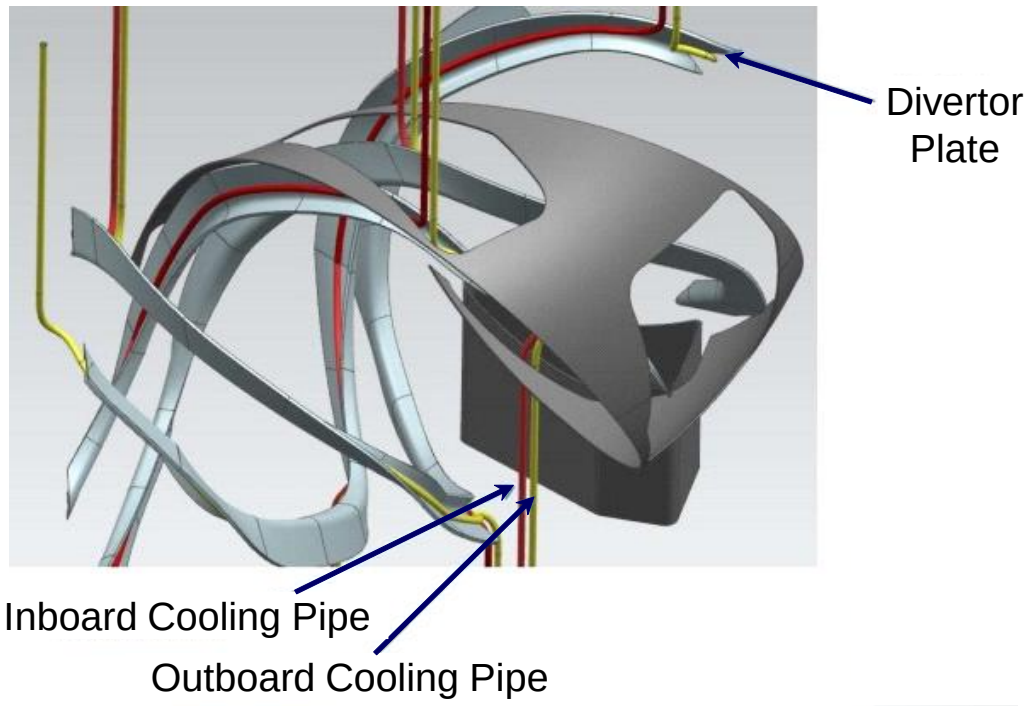

Fig. 13. Schematic illustration of the helical divertor layout.

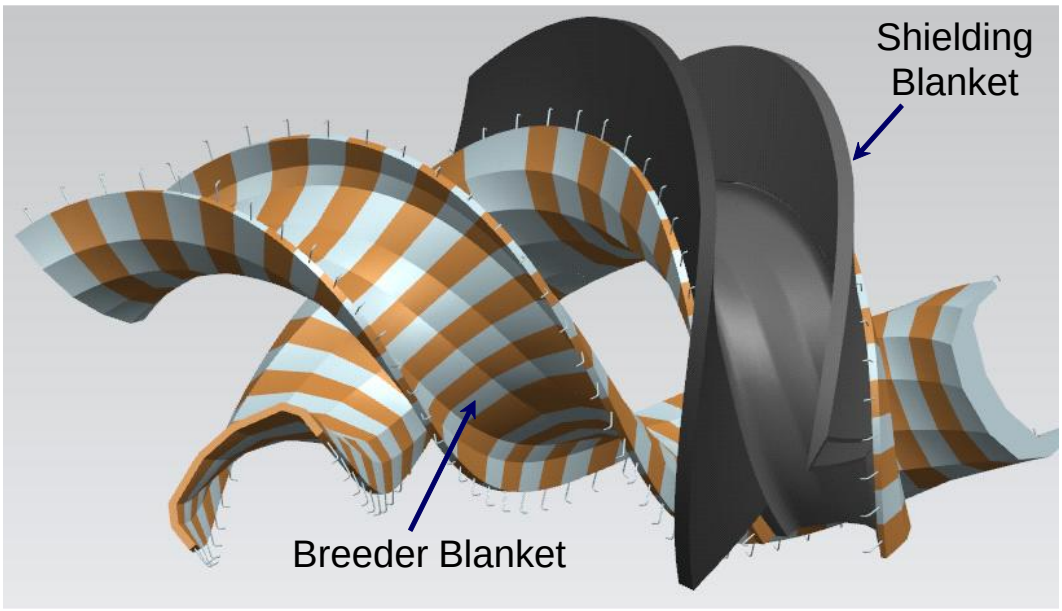

Fig. 14. Schematic illustration of the helically-segmented breeder blanket. The two colors on the breeder blanket indicate the segmentation.

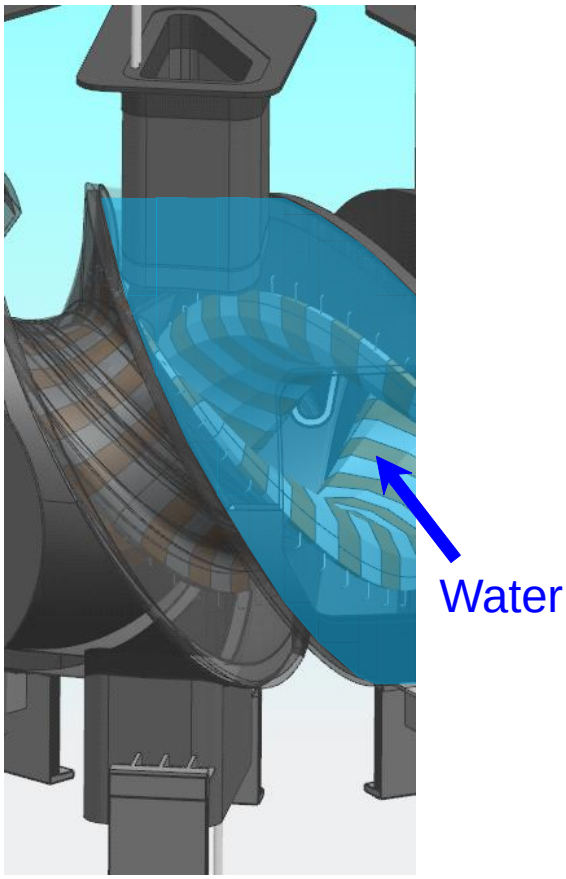

Fig. 15. Schematic illustration of the “Aquarium Method” for the maintenance of the helically-segmented breeder blanket and helical divertors by filling water into the vacuum vessel.